



ELSEVIER

Moon and Sun shadowing effect in the MACRO detector

M. Ambrosio ^a, R. Antolini ^b, A. Baldini ^c, G.C. Barbarino ^a, B.C. Barish ^d,
G. Battistoni ^{e,1}, Y. Becherini ^f, R. Bellotti ^g, C. Bemporad ^c, P. Bernardini ^h,
H. Bilokon ^e, C. Bower ⁱ, M. Brigida ^g, S. Bussino ^j, F. Cafagna ^g, M. Calicchio ^g,
D. Campana ^a, M. Carboni ^e, R. Caruso ^k, S. Cecchini ^{f,2}, F. Cei ^c, V. Chiarella ^e,
T. Chiarusi ^f, B.C. Choudhary ^d, S. Coutu ^{l,3}, M. Cozzi ^f, G. De Cataldo ^g,
H. Dekhissi ^{f,m}, C. De Marzo ^g, I. De Mitri ^h, J. Derkaoui ^{f,m}, M. De Vincenzi ⁿ,
A. Di Credico ^b, O. Erriquez ^g, C. Favuzzi ^g, C. Forti ^e, P. Fusco ^g,
G. Giacomelli ^f, G. Giannini ^{c,4}, N. Giglietto ^{g,*}, M. Giorgini ^f, M. Grassi ^c,
A. Grillo ^b, C. Gustavino ^b, A. Habig ^{o,5}, K. Hanson ^l, R. Heinz ⁱ,
E. Katsavounidis ^{d,6}, I. Katsavounidis ^{d,7}, E. Kearns ^o, H. Kim ^d, A. Kumar ^f,
S. Kyriazopoulou ^d, E. Lamanna ^{p,8}, C. Lane ^q, D.S. Levin ^l, P. Lipari ^p,
N.P. Longley ^{d,r}, M.J. Longo ^l, F. Loparco ^g, F. Maaroufi ^{f,m}, G. Mancarella ^h,
G. Mandrioli ^f, S. Manzoor ^{f,9}, A. Margiotta ^f, A. Marini ^e, D. Martello ^h,
A. Marzari-Chiesa ^s, M.N. Mazziotta ^g, D.G. Michael ^d, P. Monacelli ^k,
T. Montaruli ^g, M. Monteno ^s, S. Mufson ⁱ, J. Musser ⁱ, D. Nicolò ^c, R. Nolty ^d,
C. Orth ^o, G. Osteria ^a, O. Palamara ^b, L. Patrizii ^f, R. Pazzi ^c, C.W. Peck ^d,
L. Perrone ^h, S. Petrera ^k, V. Popa ^{f,10}, A. Rainò ^g, J. Reynoldson ^f, F. Ronga ^e,
C. Satriano ^{p,11}, E. Scapparone ^b, K. Scholberg ^{o,12}, M. Sioli ^f, G. Sirri ^f,

* Corresponding author. Tel.: +390805443163; fax: +390805534938.

E-mail address: giglietto@ba.infn.it (N. Giglietto).

¹ Also at INFN Milano, 20133 Milano, Italy.

² Also at Istituto TESRE/CNR, 40129 Bologna, Italy.

³ Also at Department of Physics, Pennsylvania State University, University Park, PA 16801, USA.

⁴ Also at Università di Trieste and INFN, 34100 Trieste, Italy.

⁵ Also at U. Minn. Duluth Physics Dept., Duluth, MN 55812, USA.

⁶ Also at Department of Physics, MIT, Cambridge, MA 02139, USA.

⁷ Also at Intervideo Inc., Torrance, CA 90505, USA.

⁸ Also at Dipartimento di Fisica dell'Università della Calabria, Rende (Cosenza), Italy.

⁹ Also at RPD, PINSTECH, P.O. Nilore, Islamabad, Pakistan.

¹⁰ Also at Institute for Space Sciences, 76900 Bucharest, Romania.

¹¹ Also at Università della Basilicata, 85100 Potenza, Italy.

¹² Also at Department of Physics, MIT, Cambridge, MA 02139, USA.

M. Sitta ^{s,13}, P. Spinelli ^g, M. Spinetti ^e, M. Spurio ^f, R. Steinberg ^q, J.L. Stone ^o,
 L.R. Sulak ^o, A. Surdo ^h, G. Tarlè ^l, V. Togo ^f, M. Vakili ^{t,14},
 C.W. Walter ^o, R. Webb ^t

^a *Dipartimento di Fisica dell'Università di Napoli and INFN, 80125 Napoli, Italy*

^b *Laboratori Nazionali del Gran Sasso dell'INFN, 67010 Assergi (L'Aquila), Italy*

^c *Dipartimento di Fisica dell'Università di Pisa and INFN, 56010 Pisa, Italy*

^d *California Institute of Technology, Pasadena, CA 91125, USA*

^e *Laboratori Nazionali di Frascati dell'INFN, 00044 Frascati (Roma), Italy*

^f *Dipartimento di Fisica dell'Università di Bologna and INFN, 40126 Bologna, Italy*

^g *Dipartimento Interateneo di Fisica del Politecnico-Università di Bari and INFN, 70126 Bari, Italy*

^h *Dipartimento di Fisica dell'Università di Lecce and INFN, 73100 Lecce, Italy*

ⁱ *Departments of Physics and of Astronomy, Indiana University, Bloomington, IN 47405, USA*

^j *Dipartimento di Fisica dell'Università di Roma Tre and INFN Sezione Roma Tre, 00146 Roma, Italy*

^k *Dipartimento di Fisica dell'Università dell'Aquila and INFN, 67100 L'Aquila, Italy*

^l *Department of Physics, University of Michigan, Ann Arbor, MI 48109, USA*

^m *L.P.T.P. Faculty of Sciences, University Mohamed I, B.P. 524 Oujda, Morocco*

ⁿ *Dipartimento di Ingegneria dell'Innovazione dell'Università di Lecce and INFN 73100 Lecce, Italy*

^o *Physics Department, Boston University, Boston, MA 02215, USA*

^p *Dipartimento di Fisica dell'Università di Roma "La Sapienza" and INFN, 00185 Roma, Italy*

^q *Department of Physics, Drexel University, Philadelphia, PA 19104, USA*

^r *Macalester College, Department of Physics and Astr., St. Paul, MN 55105, USA*

^s *Dipartimento di Fisica Sperimentale dell'Università di Torino and INFN, 10125 Torino, Italy*

^t *Physics Department, Texas A&M University, College Station, TX 77843, USA*

Received 14 February 2003; received in revised form 24 April 2003; accepted 25 April 2003

Abstract

Using data collected by the MACRO experiment from 1989 to the end of its operations in 2000, we have studied in the underground muon flux the shadowing effects due to both the Moon and the Sun. We have observed the shadow cast by the Moon at its apparent position with a significance of 6.5σ . The Moon shadowing effect has been used to verify the pointing capability of the detector and to determine the instrument resolution for the search of muon excesses from any direction of the celestial sphere. The dependence of the effect on the geomagnetic field is clearly shown by splitting the data sample in day and night observations. The Sun shadow, observed with a significance of 4.6σ is displaced by about 0.6° from its apparent position. In this case however the explanation resides in the configuration of the Solar and Interplanetary Magnetic Fields, which affect the propagation of cosmic ray particles between the Sun, and the Earth. The displacement of the Sun shadow with respect to the real Sun position has been used to establish an upper limit on the antimatter flux in cosmic rays of about 48% at 68% c.l. and primary energies of about 20 TeV.

© 2003 Elsevier B.V. All rights reserved.

PACS: 13.85.Tp; 96.40.-z; 96.40.Cd; 96.40.De; 96.40.Tv; 96.50.Bh

Keywords: MACRO; Underground muons; Moon shadowing; Sun shadowing; Geomagnetic field; IMF field; Primary antimatter

¹³ Also at Dipartimento di Scienze e Tecnologie Avanzate, Università del Piemonte Orientale, Alessandria, Italy.

¹⁴ Also at Resonance Photonics, Markham, Ontario, Canada.

1. Introduction

MACRO was a large area underground detector located in Hall B of the Gran Sasso National Laboratory (LNGS) in Italy at an average depth of 3700 m.w.e., 13°34' E longitude and 42°27' N latitude. A detailed description of the detector can be found in [1]. The experiment was primarily designed to search for monopoles and rare particles in the cosmic rays, including high energy neutrinos and muons from cosmic point sources [2]. These sources can be inferred from an excess of muons above a nearly isotropic background in a particular region of the sky [3,4]. An important requirement for any kind of detector using this technique is the determination of the best signal/background ratio, which is related to the angular resolution.

It was originally suggested by Clark [5] that an observed narrow angle “shadow” in the cosmic ray flux due to the absorption by the Sun and the Moon can be useful to test the angular resolution [6] and the pointing ability of cosmic ray detectors [3,4]. Moreover, the positive determination of the Moon shadow in the expected position, validates the analyses of coincident data between different detectors as MACRO together EAS-TOP [7] or other detectors [8].

However, since the angular diameter of these bodies is about 0.5° wide, only detectors having good angular resolution and sufficient statistics have the possibility to detect this signal. Several large air shower arrays [9–15] and shallow depth detectors [16] have observed these effects. Deep underground observations (>2000 m.w.e.) have greater difficulties in observing the shadows, due to the greatly reduced underground muon flux. However MACRO [17], SOUDAN2 [18] and LVD [19] have all collected data continuously for about 10 years, thereby gaining the sufficient sensitivity to observe the effect.

Underground muons are the remnants of the air showers initiated by the collisions of primary cosmic rays with air nuclei. The secondary muons which reach the MACRO detector had to cross a minimum rock overburden of 3200 hgcm⁻². This corresponds to a minimum energy of the muon at the surface of about 1.4 TeV and to a primary

proton with median energy around 22 TeV. Since the Earth Magnetic field is approximately (to within 10%) a dipole field, and its strength is 0.5 G at the surface, a single charged particle crossing it will acquire a transverse momentum of about 25 GeV/c for a path integral over few Earth' radii. The average displacement of muon trajectories due to this effect, as viewed in the detector, will be $[0.15^\circ Z / (E_p / 10 \text{ TeV})]$, eastward for positive primaries, [20,21]. Therefore the apparent position of the Moon shadow will appear moved to the West direction (with respect to the Earth–Moon direction) by the same amount.

The motion in time of the Earth's magnetic pole around its average position, introduces a smearing of the shadow when the effect is observed over many years [22]. Additional smearing can be produced by the fact that the observations are made at different angles and at different times of the year.

The Sun shadowing effect is more complicated to estimate. Particles shadowed by the Sun are traveling in the direction of the Sun–Earth axis and therefore are traveling through the solar magnetic field and the Interplanetary Magnetic Field (IMF). The IMF is due to the electric currents in the Sun that generate a complex magnetic field which extends out into the interplanetary space. As the Sun's magnetic field is carried out through the solar system by the solar wind and the Sun is rotating, the rotation winds up the magnetic field into a large rotating spiral, known as the Parker spiral. The magnetic field is primarily directed outward from the Sun in one of its hemispheres, and inward in the other. This causes opposite magnetic field directions in the Parker spiral. The thin layer between the different field directions is described as the neutral current sheet. Since this dividing line between the outward and inward field directions is not exactly on the solar equator, the rotation of the Sun causes the current sheet to become “wavy”, and this waviness is carried out into interplanetary space by the solar wind. For this reason the IMF shows a sector structure with field directions reversing across the sector boundaries [23,24]; therefore, in some sectors the magnetic field points inward, and outward in others. Moreover, this structure varies with the solar activity cycle; a complete simulation must

thus take into account the solar activity phase and the sectors encountered by the particle traveling in our solar system [25–27].

The possibility to use the Moon and Sun shadows as mass spectrometers was first explored by Lloyd–Evans [28]; following this idea Urban et al. [20] proposed this method as a way to search for antimatter in primary cosmic rays. If there is a significant antimatter component in the primary CRs in the TeV energy region, then the magnetic fields should deflect them in opposite direction with respect to the matter component; therefore the proton component should be deflected by the geomagnetic field eastward and the antiproton component westward. As a consequence the shadow produced by the proton component should be to the West with respect to the Moon center, while the resulting shadow due to antiprotons should be to the East. However to resolve the images, the two disks must be far from each other, at least by the disk diameter itself.

The shadow of the Moon was previously observed by MACRO using a partial data sample [17]. In this paper we present the measurement of the Moon and Sun shadows using the full data set of muons collected by the MACRO detector. Using the result obtained for the Sun we are able to set an upper limit to the antiproton flux of TeV energy at the Earth.

2. The muon data sample and the expected background

2.1. Muon data sample

The muon sample used for the present analysis includes all events collected from the start of MACRO data taking in February, 1989 through the end of 2000. The sample totals 50.0×10^6 events collected over 74,073 h of lifetime. During the first part of this period, the apparatus was under construction. The three main detector configurations included one ($A_{\text{eff}}\Omega \approx 1010 \text{ m}^2 \text{ sr}$) and six ($A_{\text{eff}}\Omega \approx 5600 \text{ m}^2 \text{ sr}$) supermodules without the attico (the upper part of the detector described in [1]), and finally the full six supermodules with at-

tico ($A_{\text{eff}}\Omega \approx 6600 \text{ m}^2 \text{ sr}$). Approximately 60% of the data sample was obtained during periods when MACRO had full acceptance.

The run and event was used to select good quality events were the same as in our first analysis of the Moon shadow [17] and for the muon-astronomy searches [3], in particular they are selected by requiring a good quality of track reconstruction based on a run-by-run analysis of the streamer and strips efficiency and event selections that remove high multiplicity events or events with zenith angles larger than 72° or events with wrong UTC times. Finally, only muon events contained in a half-angle cone of 10° and centered on the Moon and the Sun have been retained for further analysis. The number of events that passed all cuts in the Moon window was 404 988, almost doubling the previous statistics, and 396 662 events in the Sun window. The rate of accumulation of the events in the two windows is given in Fig. 1. As visible in Fig. 1 the effects of a reduced detector lifetime, due to the installation of the final configurations in years 1992–1993, produced a different exposure for the Sun and the Moon.

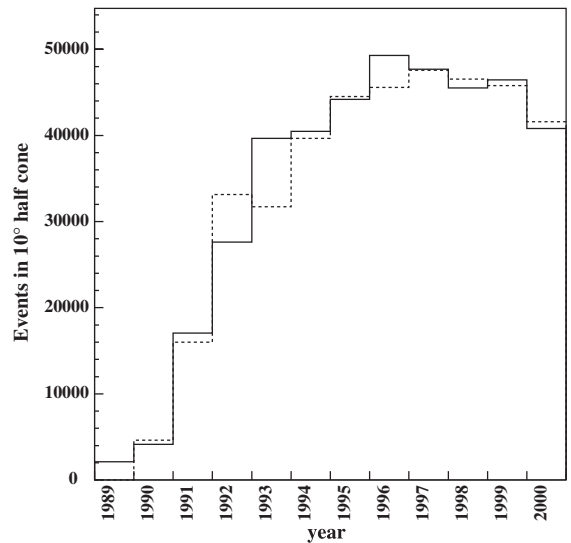


Fig. 1. Number of events in a 10° half-angle cone from the Moon direction (solid histogram) and from the Sun direction (dashed histogram) collected during each year of MACRO data taking.

We note that during the period when MACRO was operative the solar activity went from its maximum phase in 1991, through a minimum phase around 1996/97 to the beginning of the next maximum in 2001. However almost 62% of the total events were accumulated from 1994 onward, close to the period of minimum solar activity when the neutral sheet was probably lying close to the ecliptic plane with little warping [29]. The period is contained within the so-called $A > 0$ phase of the solar cycle during which the magnetic field of the Sun is directed outward at the North pole of the Sun and inward in the South.

As in our previous analysis, for each real event observed, we produced 25 simulated background events, by randomly coupling muon directions and times, as explained in [3]. This technique was used to estimate the expected events from any direction of the sky, including the Sun and the Moon.

3. Shadow of the Moon

The Moon is a celestial body moving quickly in the sky. Thus, to perform the analysis it is necessary to make a very precise and accurate computation of its position. The topocentric position of the Moon was computed at the arrival time of each event using the database of ephemerides available from the Jet Propulsion Laboratory, JPLEPH [30]. A correction for the parallax due to MACRO's instantaneous position on the Earth was then applied to each ephemeris position [31].

3.1. Event deficit around the Moon

The distribution of events with arrival directions close to the Moon direction can be used to make visible the event deficit around the Moon disk. The average disk radius is computed for each event of the 404,988 events in the sample giving a value of $(0.26 \pm 0.01)^\circ$. Fig. 2 shows the distribution $(1/\pi)(dN/d\theta^2)$ vs. θ , where θ is the angular distance between the calculated Moon center position in celestial coordinates and the muon arrival direction. The significance of the deficit can be calculated by fitting this distribution with a function of the form [9,32]:

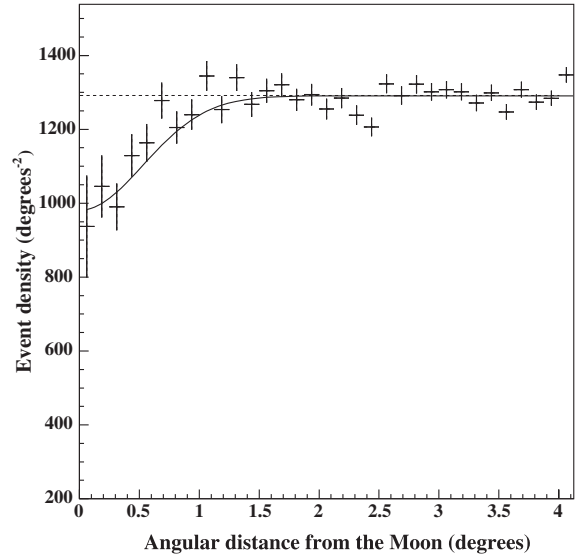


Fig. 2. Event density vs. angular distance from the Moon center in bins of equal angular width. The width of each bin is 0.125° . The dashed curve is the average expected background computed from 25 background Monte Carlo samples. The solid curve shows the expected event density computed for an angular resolution of the MACRO apparatus in the hypothesis of a PSF normally distributed. The resolution value from the fit is $0.55^\circ \pm 0.05^\circ$.

$$\frac{dN_\mu}{d\theta^2} = k \left(1 - \frac{\theta_M^2}{2\sigma^2} e^{-\frac{\theta^2}{2\sigma^2}} \right) \quad (1)$$

where $\theta_M = 0.26^\circ$ is the average value of the angular radius of the Moon, previously computed, σ is the detector angular resolution and k the event density.

This function represents the signal produced by the Moon absorption effect when the detector point spread function (PSF) can be assimilated to a bidimensional normal distribution. We know that in our case this is not really appropriate because muons observed in the apparatus undergo multiple Coulomb scattering in the overburden rock, which generates long tails in the measured angular distributions. Nonetheless, this simple analysis gives results consistent with the one presented in the next section where we take into account the real PSF of the apparatus by using a maximum likelihood method. The fit of the data to

the above function has a $\chi^2 = 54.8$ for 31 D.o.F. and a $\chi^2 = 95.9$ for a flat distribution (32 D.o.F.). The difference between these values suggests that the chance probability of the observed deficit is $\leq 10^{-9}$, equivalent to a statistical significance of about 6σ . The fitted values of the parameters are $k = (1294 \pm 5)$ events/degree² and $\sigma = (0.55 \pm 0.05)^\circ$. The value of k obtained by the fit can be used to have a rough estimate of the number of missing events (blocked by the Moon disk): $\pi k \theta_M^2 = 275 \pm 20$. We also estimated the number of missing events by considering the number of expected background events in the 10° cone windows, $N_{\text{bck}} = 405\,100 \pm 127$, calculated as mentioned above. Thus, the number of blocked events is $405,100 (0.26^\circ/10^\circ)^2 = 274 \pm 20$, in agreement with the result of the fit. Since the lifetime of the apparatus for the entire sample is about 74,000 h, the rate of the events obscured by the Moon is about 3 events/month.

The observed signal can then be used to optimize the bin size for astronomy searches [3]. In fact we can choose the size of a circular window cen-

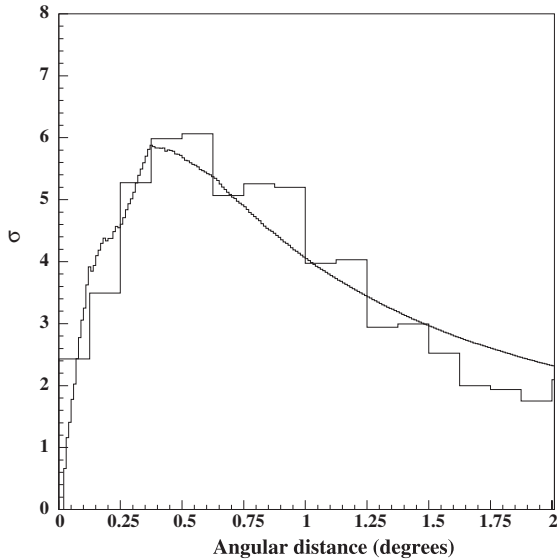


Fig. 3. Deviation from the expected number of events computed as $\sigma = (N_{\text{exp}} - N_{\text{obs}})/\sqrt{N_{\text{exp}}}$ versus the angular distance from the Moon center. Superimposed (continuous line) the simulated distribution of the deviations expected using the modified psf distribution for an extended source of 0.26° radius.

tered on the Moon that maximizes the statistics $(N_{\text{exp}} - N_{\text{obs}})/\sqrt{N_{\text{exp}}}$ integrated the number of events observed in the Moon direction and N_{exp} the integrated number of expected events in the same direction. The behavior of this quantity versus the angular distance from the Moon center, is shown in Fig. 3. This figure suggests the choice of bin 0.5° radius wide as the optimal one for maximizing the signal if there is a source at the center of the bin [3].

3.2. Maximum likelihood analysis

In the simple one dimensional analysis above, we have implicitly assumed that the position of the Moon's shadow is known and the significance calculated as the PSF of the apparatus is a perfect two dimensional normal distribution. However geomagnetic effects, displacement of the shadow and the distortions introduced by the true PSF, cannot be easily taken into account using this analysis. For all these reasons we have developed a binned likelihood method, based on a 'a priori' knowledge of the MACRO PSF (MPSF), a technique originally developed by COS-B [33].

The MPSF was accurately determined by using double muon events in the detector. Muon pair events are produced in the decays of pions and kaons produced in the primary cosmic ray interactions; these muons therefore come from about 20 km above the apparatus and have small initial separation angles; thus they reach the apparatus with almost parallel paths. Therefore, the distribution of their separation angles is a good measurement of convolution of the scattering in the mountain overburden and the detector's intrinsic angular resolution. This space angle should be divided by a factor $\sqrt{2}$ to take into account of the independent deviations of each muon in the pair. The reconstructed MPSF [17] is more peaked to small angular deviations, with respect to a normal distribution, but with long tails at large deviations. However, the reconstructed MPSF obtained, can be systematically different from the true PSF for single muons. In fact the average residual energy of underground muons result to be about 30% higher for double muons respect to single muons [34]. Thus double muons should produce a narrow

PSF respect to single muons. For this reason we have already verified in the previous work [17] and confirmed again both by likelihood analysis and the data obtained by the simulation superimposed in Fig. 3 that the MPSF obtained is compatible with the shape of the shadow observed.

In order to analyze both the Moon and the Sun shadowing effects, we have to take into account the finite size of these objects. Therefore we have modified the true MPSF by selecting random positions on a disk having the same angular dimensions of the Moon and then generating random deviations according the MPSF. This new distribution, a convolution of the original MPSF and an extended source of fixed angular radius, is then used as the PSF for the analysis. The sensitivity of the results to the angular radius of the object will be explored at the end of this section.

A two dimensional likelihood analysis was performed, composing the observed data with the expectation from a source of unknown strength and position. We filled a two-dimensional histogram, centered on the Moon position, and a similar histogram containing the simulated events, obtained by adding to the expected background [3], the events due to a source at (x_s, y_s) having a chance strength S_M , spread according to the modified PSF. The source in this case should have negative strength, since we are looking for an attenuation. Both the observed and simulated events are plotted using horizontal coordinates (azimuth and altitude) and using equal solid angle bin ($\Delta\Omega = 0.125^\circ \times 0.125^\circ = 1.6 \times 10^{-2} \text{deg}^2$). For each of the bin in the histogram used, we assume to have a source exactly at the bin center, then the unknown strength S_M is evaluated by minimizing the quantity χ^2 for Poissonian distributed data [35]

$$\chi^2(x_s, y_s, S_M) = 2 \sum_{i=1}^{n_{\text{bin}}} \left[N_i^{\text{sim}} - N_i + N_i \ln \frac{N_i}{N_i^{\text{sim}}} \right], \quad (2)$$

where the sum is over all bins in the window [35], N_i is the observed number of muons in the i th bin, and N_i^{sim} the number of events in the same bin from the simulated distribution. The minimum value found in each bin, $\chi^2(x_s, y_s, S_M)$ was then

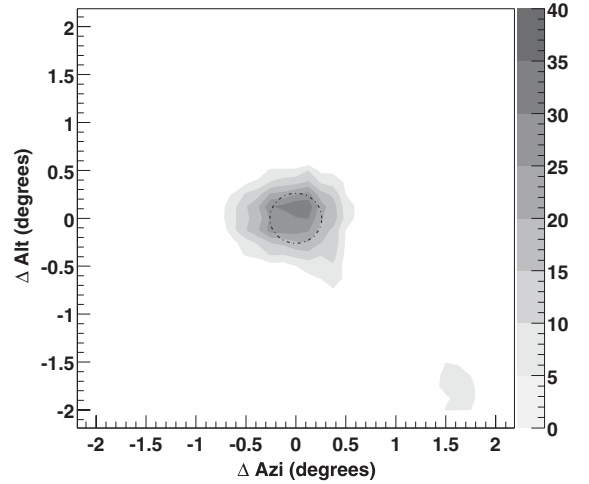


Fig. 4. The two dimensional distribution of χ^2 in bins of equal solid angle in the Moon window. The axes are offsets from the Moon center. A circle corresponding to the average lunar radius, 0.26° , is centered on the fiducial position of the Moon, at position $(0,0)$. The χ^2 grey scale is given at the right margin of the figure. The maximum of this distribution, $\chi^2 = 39.7$, is within the fiducial Moon position at $\Delta\text{Azimuth} = 0.^\circ$, and $\Delta\text{Altitude} = +0.125^\circ$. The bin width is 0.25° .

compared with $\chi^2(0)$ for the *null hypothesis* that no shadowing source is present at the center of the bin ($S_M = 0$). We then fill a new two-dimensional histogram filled with the quantity $\lambda = \chi^2(0) - \chi^2(x_s, y_s, S_M)$. The most likely position of the Moon shadow is given by the bin having the maximum value $\lambda^{\text{max}} \equiv \mathcal{A}$. Since there is only one free parameter, the strength of the source S_M , λ behaves like χ_1^2 , a χ^2 distribution with one degree of freedom [33]. The significance of the Moon detection is given by $P(\chi_1^2 \geq \chi_1^2(\mathcal{A}))$.

In Fig. 4 we show the results of this analysis in a window $4.375^\circ \times 4.375^\circ$ centered on the Moon position. This window has been divided into 35×35 cells, each having dimensions $0.125^\circ \times 0.125^\circ$. The λ values of this figure are displayed in grey scale format for every bin in the Moon window. Also shown is the fiducial position of the Moon and a circle centered at this position corresponding to the average lunar radius, 0.26° . The largest deviation away from the expected background is found at $(0.^\circ, +0.125^\circ)$ with a $\mathcal{A} = 39.1$, corresponding to a significance of 6.5σ and a

negative strength of 316 events, as expected for a shadowing effect. The χ^2 value for the null hypothesis, i.e. when a source of null intensity is set in the bin with the largest deviation found, is 1240.71 for the 35×35 bins. The entire sky region in the fiducial position of the disk has $\lambda \geq 36$ values. Moreover the negative strength observed is equal to 316 ± 40 events, in agreement with the expected deficit. The 1σ error in the strength, treated as a parameter, is directly estimated by the likelihood method by considering the parameter interval delimited by the condition $\lambda = A - 1$ [35] (or $\chi^2 = \chi_{\min}^2 + 1$).

We estimated other parameters used in the simulation like the MPSF shape itself [17], in this case to test the hypothesis that the MPSF obtained by double muons is not narrower than the true MPSF for single muons, or the Moon average radius [13], in order to verify the correctness of the analysis. For this last consideration we assume that the true shadow center position is that having the largest deviation, i.e. at $(0^\circ, +0.125^\circ)$, and repeat the analysis using different PSFs each modi-

fied by different values of the trial angular radius for the source, starting with a null value corresponding to the true, unmodified MPSF. This technique let us to both verify the sensibility of the analysis to extended PSFs and also to quote an error on the radius of the measured object. Fig. 5 shows the χ^2 values at the central shadow position, versus the trial angular disk radius. From this figure we can quote as the radius for the Moon a value of $(0.25 \pm 0.25)^\circ$, well in agreement with the correct averaged value. This result confirms that the Moon shadow signal is more likely due to an extended source instead of a point-like source.

The null displacement of the shadow observed in the West–East direction is in agreement with the expected displacement of less than 0.1° westward, thus confirming the correct alignment of the apparatus. We can quote as the maximum error in the alignment of the apparatus a value of about 0.1° , taking into account the observed shadow displacement northward.

4. Day–night effects

To study possible differences in the geomagnetic field due to the solar wind, we divided the muon sample in two subsamples by requiring that the angular distance between the Moon and the Sun is smaller or larger than 90° . This requirement is almost equivalent to a daytime–nighttime requirement on the data, similar to what was used in a previous analysis [36]. The results of the analyses for the two subsamples are shown in Fig. 6 (a and b): there is a sharper shadow for the “night” sample, with a large significance, and a broader shadow for the “day” sample (with a lower significance). Since the two subsamples are almost equivalent (198 183 and 206 805 events for “day” and “night” respectively) we conclude that night events encounter a reduced geomagnetic field with respect to the day events [37–39]. The cause has probably to be ascribed to the different configuration of the geomagnetic field in the two sides. Also time varying effects can be different for the two subsamples.

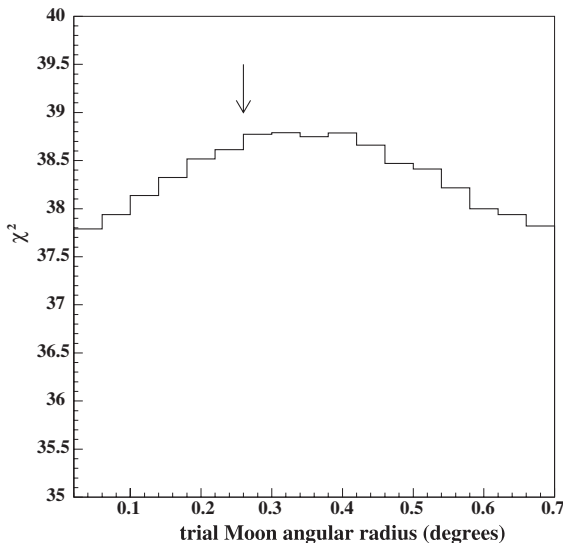


Fig. 5. Distribution of χ^2 values at the Moon shadow center versus the trial angular size for the Moon radius. The interval $\chi_{\max}^2 - 1$ establishes the error interval for the Moon angular radius. The arrow shows the expected average value for the Moon radius.

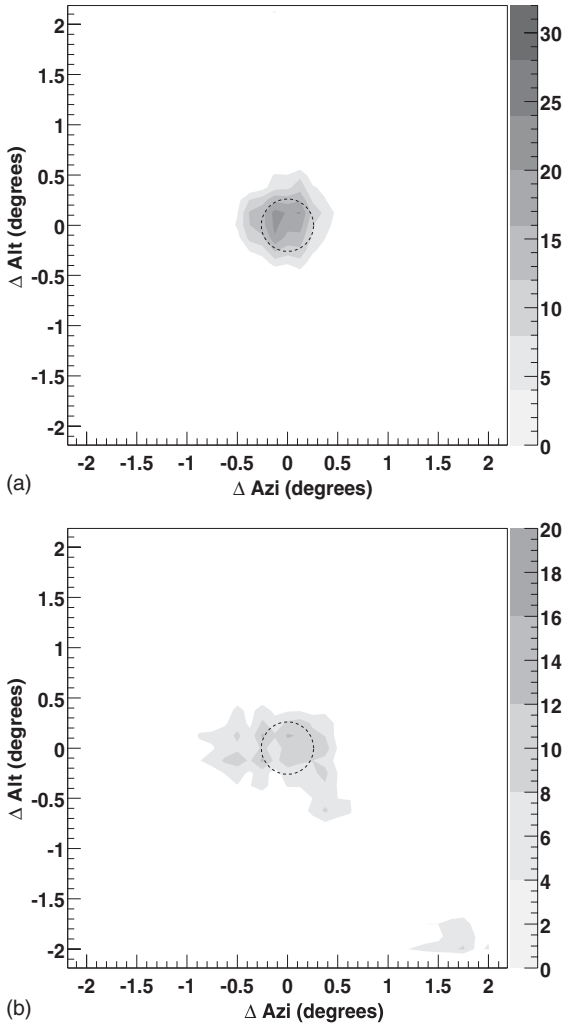


Fig. 6. The two dimensional distribution of χ^2 in bins of equal solid angle in the Moon window for the “night” (a) and “day” (b) subsamples. The axes are offsets from the Moon center. A circle corresponding to the average lunar radius, 0.26° , is centered on the fiducial position of the Moon, at position (0,0). The χ^2 grey scale is given at the right margin of the figure. (a) The maximum of the distribution, $\chi^2 = 25$, is within the fiducial Moon position at $\Delta\text{Azimuth} = -0.1^\circ$ and $\Delta\text{Altitude} = +0^\circ$. (b) The maximum of the distribution, $\chi^2 = 17.1$, at $\Delta\text{Azimuth} = -0.25^\circ$ and $\Delta\text{Altitude} = +0^\circ$.

5. Shadowing effect of the Sun

The same analysis was performed also for the Sun. In this case the total number of events collected with an angular distance from the Sun

center of 10° is 396,662, a sample almost equivalent to that of the Moon. Since the angular dimensions of the two bodies are essentially the same, we expect about the same number of missing events. However, besides the geomagnetic field effect, two other magnetic fields come into deflecting the cosmic ray particles: the Sun’s magnetic field and the IMF. As these fields are variable in time, it is more difficult to predict the shadow displacement. Using the ecliptic coordinates for the muons collected, and a window centered on the calculated Sun position, we obtain the results shown in Fig. 8. The deficit is clear and it is displaced by 0.6° northward with a $\chi^2 = 22.0$ corresponding to a signal significance of 4.6σ . The deficit observed for the Sun shadowing results to be 247 ± 48 events, using the error estimated by the likelihood method as for the Moon shadowing effect. In trying to explain our result let us analyze the behavior of the magnetic fields in the years during which we collected our data. Fig. 7 shows the monthly average A_p values [40] in the years 1989–2000. These values indicate a global (planetary) magnetic activity and are sensitive to solar particle effects on the Earth’s magnetic field. It is evident that the Sun was in a relatively quiet activity during 1993–2000, where the bulk of our events have been collected. Moreover, as we have mentioned in Section 2.1, during the whole period the solar cycle was in the so-called $A > 0$ phase. In this situation the displacement due to the large regular IMF is expected to be northward of the ecliptic plane. Let us note that from 1991 till the

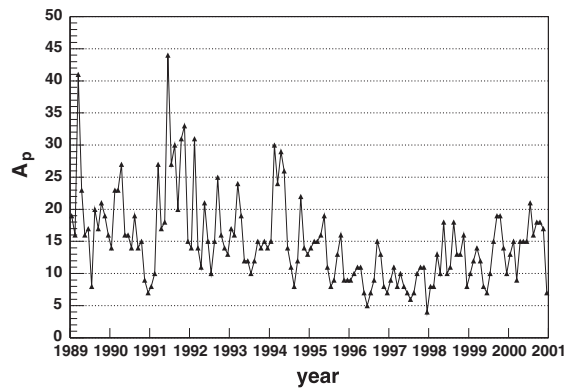


Fig. 7. Monthly A_p index in the 1989–2001 period.

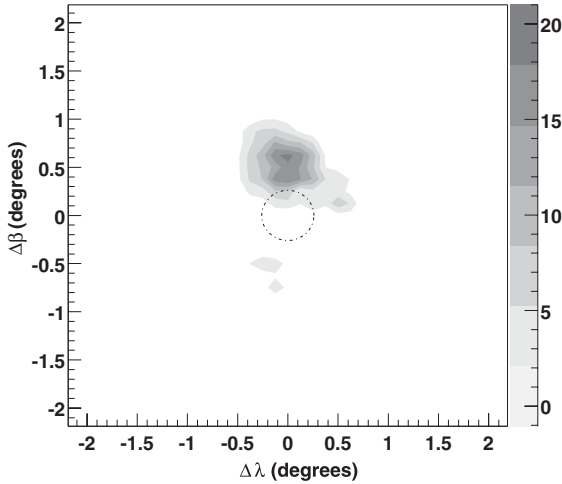


Fig. 8. The two dimensional distribution of χ^2 in bins of equal solid angle in the Sun window in ecliptic coordinates. The axes are offsets from the Sun center. A circle corresponding to the average Sun radius, 0.26° , is centered on the fiducial position of the Sun, at position (0,0). The χ^2 grey scale is given at the right margin of the figure. The maximum of this distribution, $\chi^2 = 22.0$, is in the position at $\Delta\lambda = 0^\circ$ in longitude and $\Delta\beta = +0.625^\circ$ in latitude. The bin width is 0.25° .

end of 1997 the Heliospheric Current Sheet was estimated to have a tilt angle $< 25^\circ$ and was almost symmetric between the North and South hemispheres of the solar cavity.

Since MACRO is located at a high latitude, it is possible that by averaging over a long period of observations the net result produces a displacement to the North as if the apparatus was mostly looking in the “away” hemisphere of the IMF. The amplitude and the direction of the shift is in agreement with other observations at the same energy range [41,42].

6. Antiproton flux limits

The displacement of the Sun shadow from the expected center position can be used to evaluate a limit on the antiproton abundance in the cosmic ray flux [20,22,43]. In fact, assuming that the primary cosmic rays flux producing the shadow, is mainly due to the primary protons, it is possible to search for a primary antiproton flux component looking for a shadow in the opposite direction

with respect to that of the proton flux [20]. The χ^2 level in the symmetric position with respect to the Sun center, i.e., at 0.6° southward, results to be $\chi^2 = 3.2$. In this case we use again the likelihood analysis to estimate an upper limit at the desired confidence level. Taking into account that the λ variable follows the χ^2 distribution with one degree of freedom, we can estimate the upper limit at 68% c.l. choosing $\Delta\chi^2 = 1$ and the upper limit at 90% c.l. choosing to $\Delta\chi^2 = 2.7$. Using this method we obtain $n_{68\%} = 125$ events and $n_{90\%} = 155$ events of deficit. Therefore $\bar{p}/p = 51\%$ at 68% c.l. and $\bar{p}/p = 62\%$ at 90% c.l. for primaries at a mean energy of about 20 TeV [36]. We can also evaluate the upper limit looking to the event density distributions centered in the position found for the Sun shadow, i.e. 0.6° displaced northward respect to the Sun “nominal” position, and in the symmetric position. The two distributions are shown in Fig. 9, and again is visible the deficit in the distribution northward position while the other is flat. Using the considerations derived from Fig. 3 we found that the number of observed events within 0.5° , from the distribution southward cen-

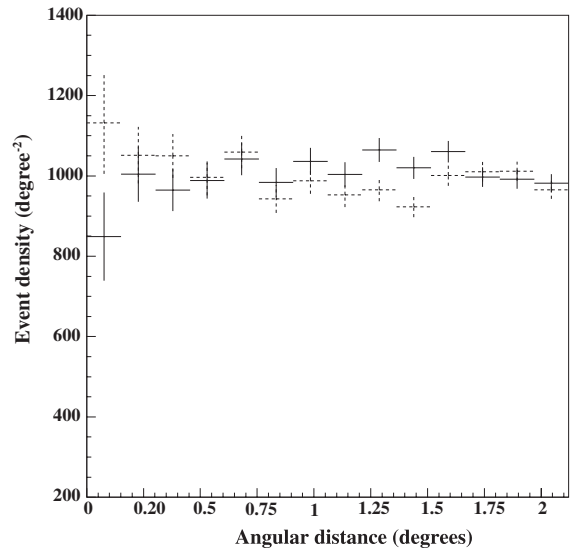


Fig. 9. Event density vs. the angular distance from the Sun shadow position (0.6° northward with respect to the “nominal center”). Superimposed (dashed line) the event density distribution centered in the symmetric position 0.6° southward respect to the Sun “nominal center”.

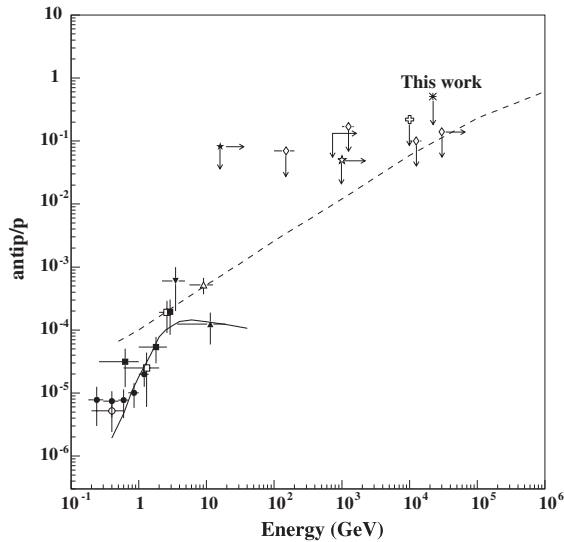


Fig. 10. Antiproton/proton ratio from various experiments at different average energies for period of $A > 0$: Δ [44]; ∇ [45]; \blacktriangle [46]; \blacksquare [47]; \circ [48]; \square [49]; \bullet [50]; \star [51]; \blackstar [52]; \diamond [53]; \dagger [36]; no symbol [16]; \ast MACRO this work. Solid line: unmodulated interstellar prediction. [54]; Dashed line: calculated anti p/p ratio for extragalactic origin [55].

tered, gives 664 events observed and 710 expected. We can therefore quote the upper limit as 60 events (68% c.l.) and 81 events (90% c.l.).

Since as previously explained [3] the choice of a 0.5° half-angle cone, collects about 50% of events from a source, the upper limit should be $\bar{p}/p = 120/247 = 48.5\%$ at 68% c.l. and $\bar{p}/p = 162/247 = 52.2\%$ at 90% c.l. in agreement with the likelihood estimations.

Fig. 10 shows our \bar{p}/p limit compared to measurements from other experiments.

7. Conclusions

Using a sample of 50 million muons MACRO has detected the Moon and Sun shadows, with a significance of 6.5σ and 4.6σ , respectively. The strength of the signals is in agreement with those expected. The Moon shadow effect is centered as expected in the case of primary protons of 15 TeV energy (median), demonstrating the correctness and the stability of the detector pointing ability.

The Sun shadow is shifted with respect to the “nominal” center position. The absence of a symmetric shadow leads to an upper limit of the \bar{p}/p ratio of 48.5% at 68% c.l. for high energy cosmic rays. MACRO is the deepest detector to observe the shadows of the Sun and of the Moon. This investigation confirms that the apparatus had the capability to detect signals from cosmic sources by observing secondary muons underground [3,4].

Acknowledgements

We gratefully acknowledge the support of the director and of the staff of the Laboratori Nazionali del Gran Sasso and the invaluable assistance of the technical staff of the Institutions participating in the experiment. We thank the Istituto Nazionale di Fisica Nucleare (INFN), the US Department of Energy and the US National Science Foundation for their generous support of the MACRO experiment. We thank INFN, ICTP (Trieste), WorldLab and NATO for providing fellowships and grants (FAI) for non-Italian citizens.

References

- [1] MACRO Collaboration, S.P. Ahlen et al., *Nucl. Instrum. Meth. A* 324 (1993) 337; MACRO Collaboration, M. Ambrosio et al., *Nucl. Instrum. Meth. A* 486 (2002) 663.
- [2] MACRO Collaboration, M. Ambrosio et al., *hep-ex/0206027*.
- [3] MACRO Collaboration, S. Ahlen et al., *Astrophys. J.* 412 (1993) 301; MACRO Collaboration, M. Ambrosio et al., *Astrop. Phys.* 18 (2003) 615.
- [4] MACRO Collaboration, M. Ambrosio et al., *Astrophys. J.* 546 (2001) 1038.
- [5] G.W. Clark, *Phys. Rev.* 108 (1957) 450.
- [6] M. Merck et al., *Astrop. Phys.* 5 (1996) 379.
- [7] MACRO-EAS TOP Collaborations, M. Aglietta et al., *Phys. Lett. B* 337 (1994) 376; *Phys. Rev. D* 42 (1990) 1396.
- [8] MACRO-GRACE Collaborations, M. Ambrosio et al., *Phys. Rev. D* 50 (1994) 3046.
- [9] D.E. Alexandreas et al., *Phys. Rev. D* 43 (1991) 1735.
- [10] P.L. Ghia et al., in: O. Fackler, G. Fontaine, J. Trân Thanh Vân (Eds.), *Proceedings of the 26th Rencontres de Moriond*, Edition Frontières, 1991, p. 217; *Proceedings of the 22nd ICRC*, Dublin, 1991, vol. 2, p. 708.

- [11] A. Karle et al., Proceedings of the 22nd ICRC, Dublin, 1991, vol. 4, p. 460.
- [12] M. Amenomori et al., Phys. Rev. D 47 (1993) 2675.
- [13] A. Borione et al., Phys. Rev. D 49 (1994) 1171.
- [14] F. Samuelson et al., Proceedings of the 27th ICRC, Hamburg, 2001, vol. 2, p. 594.
- [15] B. Bartoli et al., Nuovo Cim. 24C (2001) 669.
- [16] L3 Collaboration, J. Parriaud, in: Proceedings of XIVth Rencontres de Blois, 2002. Available from <arXiv:astro-ph/0210334>, in press.
- [17] MACRO Collaboration, M. Ambrosio et al., Phys. Rev. D 59 (1999) 012003; MACRO Collaboration, N. Giglietto et al., in: Proceedings of the 26th ICRC, Salt Lake City, 1999, vol. 7, p. 214.
- [18] J.H. Cobb et al., in: Proceedings of the 26th ICRC, Salt Lake City, 1999, vol. 7, p. 230.
- [19] LVD Collaboration, M. Aglietta et al., in: Proceedings of the 26th ICRC, Salt Lake City, 1999, vol. 7, p. 22.
- [20] M. Urban et al., Nucl. Phys. Proc. Suppl. 14B (1990) 223.
- [21] J. Heintze et al., MPI-H-1989-V7 and Proceedings of the 21st ICRC, Adelaide, 1990, vol. 4, p. 456.
- [22] D. Pomarède et al., Astrop. Phys. 14 (2001) 287.
- [23] J.M. Wilcox, N.F. Ness, J. Geophys. Res. 70 (1965) 5783.
- [24] L. Svalgaard, J.M. Wilcox, Ann. Rev. Astron. Astrophys. 16 (1978) 429.
- [25] M. Onhishi et al., Proceedings of the 22nd ICRC, Dublin, 1991, vol. 2, p. 69.
- [26] T. Zhang, J. Mu, in: Proceedings of the 26th ICRC, Salt Lake City, 1999, vol. 7, p. 210.
- [27] Y. Suga et al., in: Proceedings of the 26th ICRC, Salt Lake City, 1999, vol. 7, p. 202.
- [28] J. Lloyd-Evans, in: Proceedings of the 19th ICRC, La Jolla, 1985, vol. 2, p. 173.
- [29] A. Balogh, E.J. Smith, Space Sci. Rev. 97 (2001) 147.
- [30] E.M. Standish et al., JPL planetary and lunar ephemerides, JPL IOM 314 (1995) 10.
- [31] P. Duffett-Smith, Practical Astronomy with your Calculator, Third ed., Cambridge University Press, 1988, p. 150.
- [32] J.H. Cobb et al., Phys. Rev. D 61 (2000) 092002.
- [33] A.M.T. Pollock et al., Astron. Astrophys. 94 (1981) 116.
- [34] MACRO Collaboration, M. Ambrosio et al., Astrop. Phys. 19 (2003) 313.
- [35] D.E. Groom et al., Eur. Phys. J. C 15 (2000) 1.
- [36] M. Amenomori et al., in: Proceedings of the 25th ICRC, Rome, 1995, vol. 4, p. 1148.
- [37] N.A. Tsyganenko, J. Geophys. Res. 100 (1995) 5599.
- [38] N.A. Tsyganenko, D.P. Stern, J. Geophys. Res. 101 (1996) 27187.
- [39] X.-W. Zhou et al., Geophys. Res. Lett. 24 (1997) 1451.
- [40] J. Bartels et al., J. Geophys. Res. 44 (1939) 411. Available from <http://www.ngdc.noaa.gov/stp/GEOMAG/kp_ap.html>.
- [41] M. Amenomori et al., Astrophys. J. 464 (1996) 954.
- [42] M. Amenomori et al., Astrophys. J. 541 (2000) 1051; M. Amenomori et al., in: Proceedings of the 27th ICRC, Hamburg, 2001, vol. 9, p. 3795.
- [43] M. Chantell et al., Nature 367 (1994) 25.
- [44] R.L. Golden et al., Phys. Rev. Lett. 43 (1979) 1196.
- [45] E.A. Bogomolov et al., in: Proceedings of the 16th ICRC Kyoto, 1979, vol. 1, p. 330.
- [46] MASS Collaboration, M. Hof et al., Astrophys. J. 467 (1996) L33.
- [47] IMAX Collaboration, J.W. Mitchell et al., Phys. Rev. Lett. 87 (1996) 3057.
- [48] BESS Collaboration, K. Yoshimura et al., Phys. Rev. Lett. 75 (1995) 3792; BESS Collaboration, A. Misseev et al., Astrophys. J. 474 (1997) 479.
- [49] CAPRICE Collaboration, M. Boezio et al., Astrophys. J. 487 (1997) 415.
- [50] BESS Collaboration, H. Matsunaga et al., Phys. Rev. Lett. 81 (1998) 4052.
- [51] G. Brooke, A.W. Wolfendale, Nature 202 (1964) 480.
- [52] N. Durgaprasad, P.K. Kunte, Nature 234 (1971) 74.
- [53] S.A. Stephens, Astron. Astrophys. 149 (1985) 1.
- [54] S.H. Geer, D.C. Kennedy, Astrophys. J. 532 (2000) 648.
- [55] S.A. Stephens, R.L. Golden, Space Sci. Rev. 46 (1987) 31.